


RESEARCH ARTICLE

Effects of glass–ceramic produced by the sol–gel route in macrophages recruitment and polarization into bone tissue regeneration

Raquel Barroso Parra da Silva¹ | Claudia Cristina Bigueti² | Marcelo Salles Munerato³ | Renato Luis Siqueira⁴ | Edgard Dutra Zanotto⁴ | Guilherme Halawa Abu Kudo³ | Gustavo Baroni Simionato¹ | Ana Carolina Zucon Bacelar¹ | Rafael Carneiro Ortiz⁵ | Joel Santiago Ferreira-Junior³ | Idelmo Garcia Rangel-Junior⁶ | Mariza Akemi Matsumoto¹ 

¹Department of Basic Sciences, São Paulo State University (Unesp), School of Dentistry, Araçatuba, Brazil

²Regenerative Medicine Laboratory, School of Podiatric Medicine, The University of Texas Rio Grande Valley – UTRGV, Harlingen, Texas, USA

³Department of Health Sciences, Centro Universitário Sagrado Coração, Bauru, Brazil

⁴Department of Material Engineering, São Carlos Federal University, São Paulo, Brazil

⁵Hospital for Rehabilitation of Craniofacial Anomalies, University of São Paulo, Bauru, Brazil

⁶Department of Diagnosis and Surgery, São Paulo State University (Unesp), School of Dentistry, Araçatuba, Brazil

Correspondence

Mariza Akemi Matsumoto, Department of Basic Sciences, São Paulo State University (Unesp), School of Dentistry, José Bonifácio Street 1193, Araçatuba 16015-050, Brazil. Email: mariza.matsumoto@unesp.br

Funding information

Fundação de Amparo à Pesquisa do Estado de São Paulo, Grant/Award Number: 2016/03762-7

Abstract

Effective bone substitute biomaterials remain an important challenge in patients with large bone defects. Glass ceramics produced by different synthesis routes may result in changes in the material physicochemical properties and consequently affect the success or failure of the bone healing response. To investigate the differences in the orchestration of the inflammatory and healing process in bone grafting and repair using different glass–ceramic routes production. Thirty male Wistar rats underwent surgical unilateral parietal defects filled with silicate glass–ceramic produced by distinct routes: BS – particulate glass–ceramic produced via the fusion/solidification route, and BG – particulate glass–ceramic produced via the sol–gel route. After 7, 14, and 21 days from biomaterial grafting, parietal bones were removed to be analyzed under H&E and Massons' Trichome staining, and immunohistochemistry for CD206, iNOS, and TGF- β . Our findings demonstrated that the density of lymphocytes and plasma cells was significantly higher in the BS group at 45, and 7 days compared to the BG group, respectively. Furthermore, a significant increase of foreign body giant cells (FBGCs) in the BG group at day 7, compared to BS was found, demonstrating early efficient recruitment of FBGCs against sol–gel-derived glass–ceramic particulate (BS group). According to macrophage profiles, CD206⁺ macrophages enhanced at the final periods of both groups, being significantly higher at 45 days of BS compared to the BG group. On the other hand, the density of transformation growth factor beta (TGF- β) positive cells on 21 days were the highest in BG, and the lowest in the BS group, demonstrating a differential synergy among groups. Noteworthy, TGF- β ⁺ cells were significantly higher at 21 days of BG compared to the BS group. Glass–ceramic biomaterials can act differently in the biological process of bone remodeling due to their route production, being the sol–gel route more efficient to activate M2 macrophages and specific FBGCs compared to the traditional route. Altogether, these features lead to a better understanding of the effectiveness of

inflammatory response for biomaterial degradation and provide new insights for further preclinical and clinical studies involved in bone healing.

KEYWORDS

biomaterial, bone repair, glass-ceramic, inflammation, M2 macrophages, sol-gel route

1 | INTRODUCTION

Bone defects resulting from malformation, infection, trauma, or tumor resection remain a significant challenge in dental, orthopedic, and craniofacial surgery. This challenge primarily arises from the size of these defects, which often surpass the natural regenerative capacity of bone.^{1,2} The field has seen a growing utilization of various bone substitute biomaterials and autogenous bone grafts as effective strategies for craniofacial reconstruction.^{3,4} Biomaterials are favored over autogenous bone due to their potential to obviate the need for additional surgical procedures and the associated morbidities.^{5,6} Among the potent autogenous bone substitutes, bioactive biomaterials, particularly those based on hydroxyapatite (HA), alpha or beta-tricalcium phosphate, biphasic calcium phosphate, bioactive glasses, and glass-ceramics, have demonstrated robust bone bioactivity.^{7,8}

A myriad of processing techniques has been applied to the development of bioactive glasses and related glass-ceramics. These techniques aim to enhance biocompatibility and bioactivity for effective bone healing while minimizing the risk of biomaterial implantation failure.⁹⁻¹⁷ Glass biomaterials are predominantly fabricated using either traditional solidification (BS) or sol-gel processes (BG), involving heating the bioactive glass beyond its crystallization temperature, typically ranging from 610 to 630°C.¹⁸ Crystallization in melt-derived glasses results in a reduction of the parent glass's microstructure and porosity, leading to solidification and subsequent physical stress.¹⁹ Sol-gel methods exhibit a distinct behavior upon liquid contact, with the biomaterial's porous structure absorbing a certain amount of liquid.²⁰ A recent study by Fiume et al. introduces a novel sol-gel methodology for developing bioactive silicate scaffolds that exhibit enhanced bioactivity in simulated body fluid. Interestingly, this research highlights variations in bioactivity even within similar glass-ceramic compositions, emphasizing the need for an accessible and reproducible manufacturing strategy to enhance bone healing using glass-ceramic-derived biomaterials.²¹

At the cellular level, biomaterials based on the sol-gel method can achieve a greater surface area, promoting enhanced bioactivity of glass materials, likely due to the formation of small pores on their surface and the high concentration of silanol groups.²² Specifically, Biosilicate[®] particles synthesized via the sol-gel route (BG) exhibit an increase in specific surface area from 0.51 to 3.01 m²/g, pore volume from 0.0005 to 0.0025 cm³/g, and average pore diameter from 4.31 to 6.16 nm. This leads to greater availability of the hydroxycarbonate surface.²³ Interactions between distinct routes produced by particulate glass-ceramic biomaterials with cells in the injury microenvironment are crucial to evoke a specific and regulated immune-inflammatory

response.²⁴ Therefore, rapid biomaterial recognition is expected, followed by spontaneous protein adsorption on its surface, minimizing excessive inflammation.²⁵

During fracture healing, recruitment of monocyte/macrophage lineage is crucial for effective functional orchestration of tissue repair.²⁶ These cells play a pivotal role in recognizing biomaterials from the protein layer, ultimately leading to cell activation²⁷ and regulation of inflammatory response.²⁸ Furthermore, macrophages possess significant polarization capacity, adopting pro- and anti-inflammatory phenotypes (M1 and M2, respectively), and secreting diverse cytokines and chemokines guiding the healing process at the implanted site.²⁹ The balance between M1/M2 phenotypes has been linked to the success or failure of biomaterial integration, influencing bone healing or persistent inflammation and fibrosis, primarily depending on biomaterial characteristics.²⁹

Classic macrophage polarization toward the M1 profile is triggered by interaction with local pro-inflammatory signals like microbial products (LPS) and interferon-gamma (IFN-γ).^{30,31} Conversely, M2 macrophages are activated by anti-inflammatory molecules secreted by platelets, blood clot products, and leukocytes, such as interleukins (IL) IL-4, IL-10, and IL-13, as well as transforming growth factor beta (TGF-β).^{32,33} However, to date, there have been no investigations in vivo models of biomaterial grafting to evaluate the efficiency of the sol-gel method compared to particulate glass-ceramic produced via solidification concerning the biological behavior of local inflammatory cells. Throughout the bone healing process, resident and inflammatory cells also induce the formation of foreign body giant cells (FBGCs) through monocyte fusion, contributing to biomaterial degradation.³⁴⁻³⁶ Despite FBGCs often being associated with fibrosis and encapsulation of biomaterials, Trindade et al. demonstrated an important role of FBGCs in bone formation, releasing anti-inflammatory factors like TGF-β.³⁶

Expanding upon our prior research, the current study aimed to explore disparities between granulated glass-ceramic materials generated via the sol-gel route and the conventional solidification route, focusing on their capacity to modulate pro-osteogenic cellular responses in an in vivo setting. Initially, we assessed the impact of BS and BG on general inflammatory cells, bone tissue, and biomaterials through histological sections. Subsequently, we compared the duration of bone healing following BS or BG grafting, considering the prevalence of M1 and M2 macrophage phenotypes, along with their associated osteoconductive capabilities. Coupled with our earlier findings, these novel insights into the therapeutic implications of BS and BG glass-ceramics in facilitating pro-osteogenic processes via activation/recruitment of macrophage phenotypes will offer significant perspectives for refining biomaterial design in the field of bone tissue engineering.

2 | MATERIALS AND METHODS

2.1 | Animal and experimental design

All experimental protocols followed the National Institutes of Health (NIH) guidelines for animal care and were approved by the Institutional Animal Care And Use Committee at the Sagrado Coração University (protocol 2664030417). Thirty male Wistar rats (*Rattus norvegicus*) aged 90 days, and mean weight of 3500 grams were provided by the Central Animal House of Unisagrado (Centro Universitário Sagrado Coração, Bauru, SP, Brazil). The rats were kept in groups of three in polypropylene cages (1394 cm²) in a room under controlled temperature (22 ± 2°C) with 12 h dark/light cycle, humidity of 40% to 70%, and received water and pelleted diet (Nuvelab CR-1, Nuvital Nutrientes S/A, Colombo, PR, Brazil) ad libitum.

2.2 | Surgical procedures

Animals were randomly divided into two groups that underwent surgical procedures for the calvaria implantation of BS (Biosilicate[®], #WO 2004/074199, 180–212 μm, Vitrovita, São Carlos, Brazil), and BG (Biosilicate Sol-Gel, #WO 2004/074199, 180–212 μm, Vitrovita, São Carlos, Brazil) glass-ceramics.^{23,37} Surgical protocol and post-surgical animal care were performed as previously described.³⁸ Briefly, animals were anesthetized by intramuscular injection of 1% ketamine (Dopalen[®], Agribands Ltda, São Paulo, Brazil) with 2% chlorite of xylazine (Anasedan[®], Agribands Ltda, São Paulo, Brazil). Then, a front-parietal trichotomy and disinfection with 1% polyvinylpyrrolidone were performed, followed by a 5 mm thickness defect in the parietal bones using a trephine bur (Neodent[®], Curitiba, Brazil) under constant saline solution irrigation.

Following biomaterial grafting, equivalent amount of the biomaterials was used, 0.02 g, agglutinated with 0.9% saline solution to fill in the bone defects. Periosteum was repositioned and the skin was sutured with 6-0 nylon. The animals received two doses of 40.000UI benzathine penicillin IM every 48 h. At the post-surgical time points of 7, 21, and 45 days, animals were sacrificed with an overdose of a ketamine/xylazine mixture and, the cranial structures were collected, and fixed in 4% formalin for 48 h. Next, specimens were washed in tap water for 12 h to be processed for microscopic analysis (H&E, Masson Trichrome, and immunohistochemistry).

2.3 | Histopathological and histomorphometry analysis

Cranium samples were demineralized in EDTA solution containing 4.13% tritriplex III (Merck KGaA, Darmstadt, Germany), and 0.44% sodium hydroxide, for approximately 40 days and embedded in Histosec[®] (paraffin enriched with polymers of the EMD Millipore-division of Merck KGaA, Darmstadt, Germany). Coronal semi-serial

5-μm thickness sections (intervals of 200 μm) were made for histologic (H&E and Masson Trichrome) and immunostaining analysis, as previously described.³⁹ Each histopathological qualitative assessment was separately evaluated by a pathologist (MAM) blinded to the groups. Quantitative assessments were made in terms of local biomaterial, resident, and inflammatory cells, which include residual blood clots, neutrophils (polymorphonuclear leukocytes, PMN), lymphocytes and plasma cells (mononuclear leukocytes, MN), foreign body giant cells (FBGC), fibers, fibroblasts, and blood vessels. Additionally, bone cells and matrix were also analyzed at sites of biomaterial implantation.

For this purpose, three histological fields at ×40 magnification were captured, comprising two peripheral and two center areas of bone defect, and submitted to a 398 points grid in a quadrangular area, by using ImageJ software (Version 1.51, National Institutes of Health). Results were normalized by the area density (%) of each parameter, considering 398 points as 100% of the area.

2.4 | Immunostaining analysis

Immunohistochemistry was performed based on previous studies for the detection of M1 and M2 macrophages during bone healing with distinct glass-ceramic (BS and BG).⁴⁰ Slides were deparaffinized by xylol and rehydrated by different concentrations of alcohol, followed by endogenous peroxidase and serum proteins blockade. Then, polyclonal primary antibodies incubation was made overnight for F4/80 (sc-26643-R), iNOS2 (sc-649), CD206 (sc-34577), and TGF-β (sc-7892) (Santa Cruz Biotechnology, Dallas, TX, USA). All primary antibodies were conjugated for 25 min with HRP-polymer (Easy Link One, EasyPath, Immunobioscience Corp., Mukilteo, USA), except by CD206 which was conjugated with Immpress/HRP (Vector Labs, Southfield, USA). Visualization was performed using 3,30-diaminobenzidine tetra hydrochloride (SigmaAldrich, St Louis, USA) and counter-stained with Mayers' hematoxylin. For negative controls, primary antibodies were substituted by Tris-buffered saline (TBS). For quantification, five fields under 40× magnification were captured by a light microscopy (Nikon, Tokyo, Japan), and a 391-point grid was used at ImageJ software. The results were normalized by the area density (%) of each parameter, considering 391 points as 100% of the area.

2.5 | Statistical assessment

Statistical tests were performed with GraphPad Prism 6.0 software (GraphPad Software Inc.). Comparisons between two groups were performed using Student's t-test for data normal distribution and using Mann-Whitney (Wilcoxon rank-sum test) for data with non-normal distribution. Multiples comparisons with normal distribution were analyzed by One-way analysis of variance (ANOVA), followed by Tukey's post hoc test. Values of $p < .05$ were considered statistically significant.

3 | RESULTS

3.1 | Histopathological analysis

Morphological analysis of H&E and Masson Trichrome revealed that in BS group, sparsely large irregular granules particles were identified among newly formed capillaries, and the granulation tissue, followed by focal osteogenic activity at the periphery of the defect (Figure 1A). Besides that, focal and scarce PMN, and MN could be seen into collagen fibers and surrounding BS, which exhibited close contact with thin and long-shaped FBGCs at 7 days (Figure 1C,D). For BG group, morphological analysis demonstrated that in initial period of 7 days, calvaria's defect was composed by small homogenous rounded BG

granules compared to BS granules (Figure 1B). This area exhibited several MN and small rounded FBGCs were found among BG granules (Figure 1E). Furthermore, a full composition of the BG with low cellularity, and slight collagen fibers, which can also be observed in Masson's Trichrome (Figure 1F).

At day 21, osteogenic activity increased peripherally while BS' granules presented focal degradation, characterized by the loss of their original shape and accumulation of FBGCs involvement (Figure 1G). Additionally, extracellular matrix presents maturation, characterized by more defined vascularization and collagen fibers maturation compared to initial period (Figure 1I,J). A decrease of BG granules promoted by resorption at period of 21 days was accomplished by the increase of FBGCs associated to the biomaterial was noted (Figure 1H).

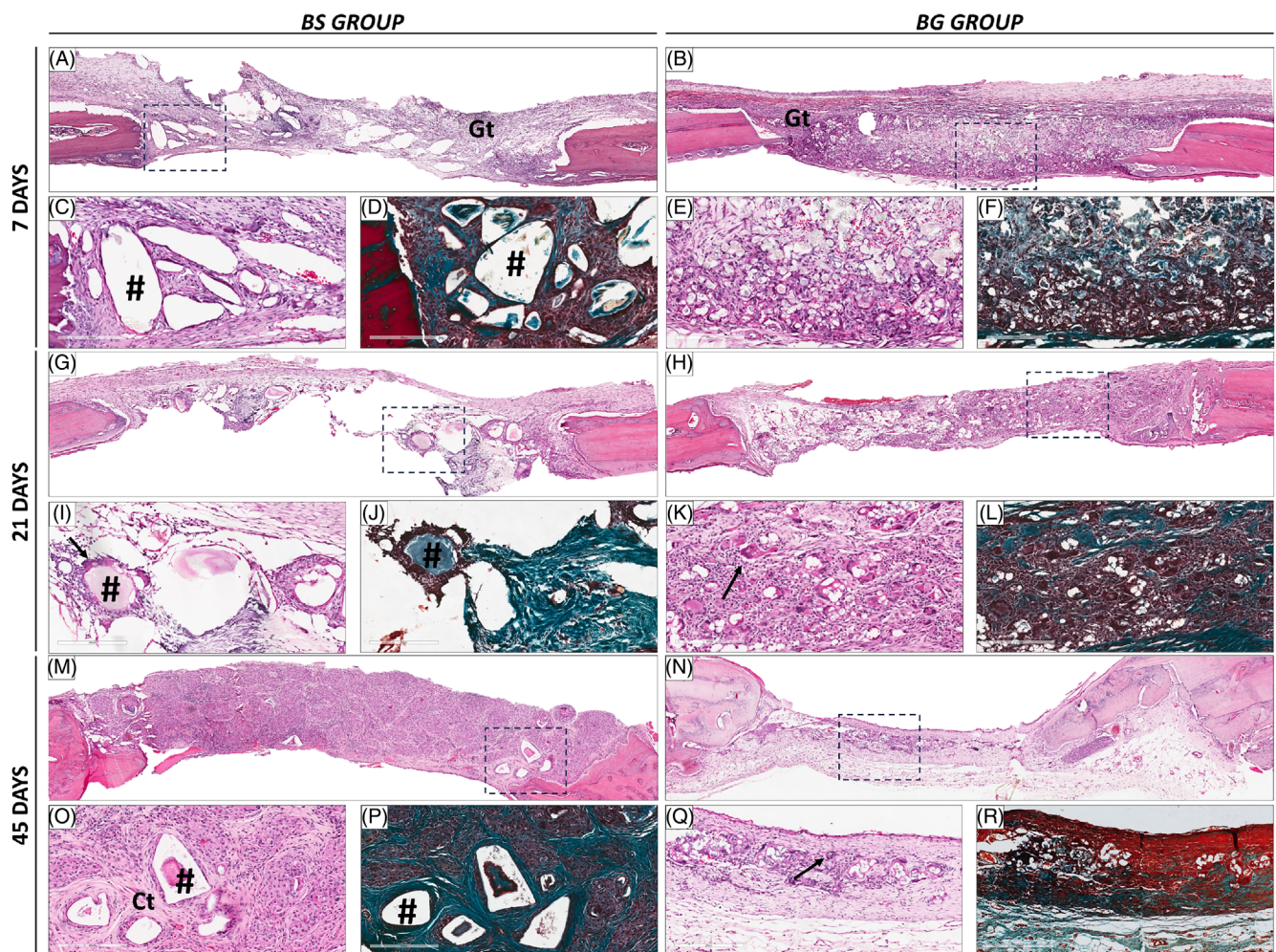


FIGURE 1 Morphological analysis of H&E and Masson Trichrome on healing defects reconstructed with BS and BG groups. Bone defect reconstructed with BS biomaterial (#) at (A) 7, (G) 21, and (M) 45 days demonstrating focal and scarce PMN, and MN (C) into collagen fibers (D) surrounded by BS, and (I, F) closely in contact with FBGCs (black arrow) at 21 days. (O, P) Extracellular matrix presents maturation, exhibiting a higher concentration of MN in close contact with scarce reminiscent biomaterial. Bone defect reconstructed with BG biomaterial (#) at (B) 7, (H) 21, and (N) 45 days demonstrating (E, F) MN and small rounded FBGCs among BG granules. Decreased of BG granules at 21 days, followed by (K, L) changes in the FBGCs' morphology, similar to Langhan's giant cells. (Q, R) An increasing in collagen maturation, and numerous FBGCs and MNs surrounding focal biomaterial granules at 45 days was observed in BG group. Gt indicates granulation tissue and Ct means connective tissue. Original magnification 4× (A-B, G-H, and M-N) and 40× (C-D, E-F, I-J, K-L, O-P, and Q-R).

MN was also present at this period, however a presence of chronic inflammation, and increasing in collagen maturation were identified (Figure 1K,L).

Finally, a higher concentration of MN in close contact with scarce reminiscent biomaterial was observed at day 45 in BS group (Figure 1M,O,P). At day 45 for BG group, discrete increased in osteogenic activity was observed in peripheral areas of biomaterial implantation, as well as a high density of collagen fibers (Figure 1N). Among these structures, numerous FBGCs and MNs were observed surrounding focal biomaterial granules of the biomaterial. It was possible to note in BG group, especially after the period of 21 days, changes in the FBGCs' morphology, similar to Langhan's giant cells, characterized by the nuclei lined up along one edge of the cell, and mostly surrounded by macrophages are elongated with long, pale nuclei and pink cytoplasm macrophages (Figure 1O,R).

3.2 | Quantitative assessment of histological parameters

To identify potential factors and cells that induce pro- or anti-inflammatory activation in response to BS and BG groups culminating to success or failure in bone repair, we evaluated the presence of PMN, MN, FBGCs, bone area and, extracellular matrix components (fibroblasts and collagen fibers) at 7, 21, and 45 days after implantation. No statistically significant differences were detected considering PMN between BS and BG groups in all experimental periods (Figure 2A). However, the percentage of MN was high in 45 days compared to 7, and 21 days, respectively. Following experimental period, MN was high in 7 days compared to 21 days. Also, the area density of MN was significant higher in BS group at 45 (3.82 ± 1.16 vs. 2.74 ± 0.96 ; $p < .05$), and 7 (1.61 ± 0.76 vs. 0.56 ± 0.46 ; $p < .05$)

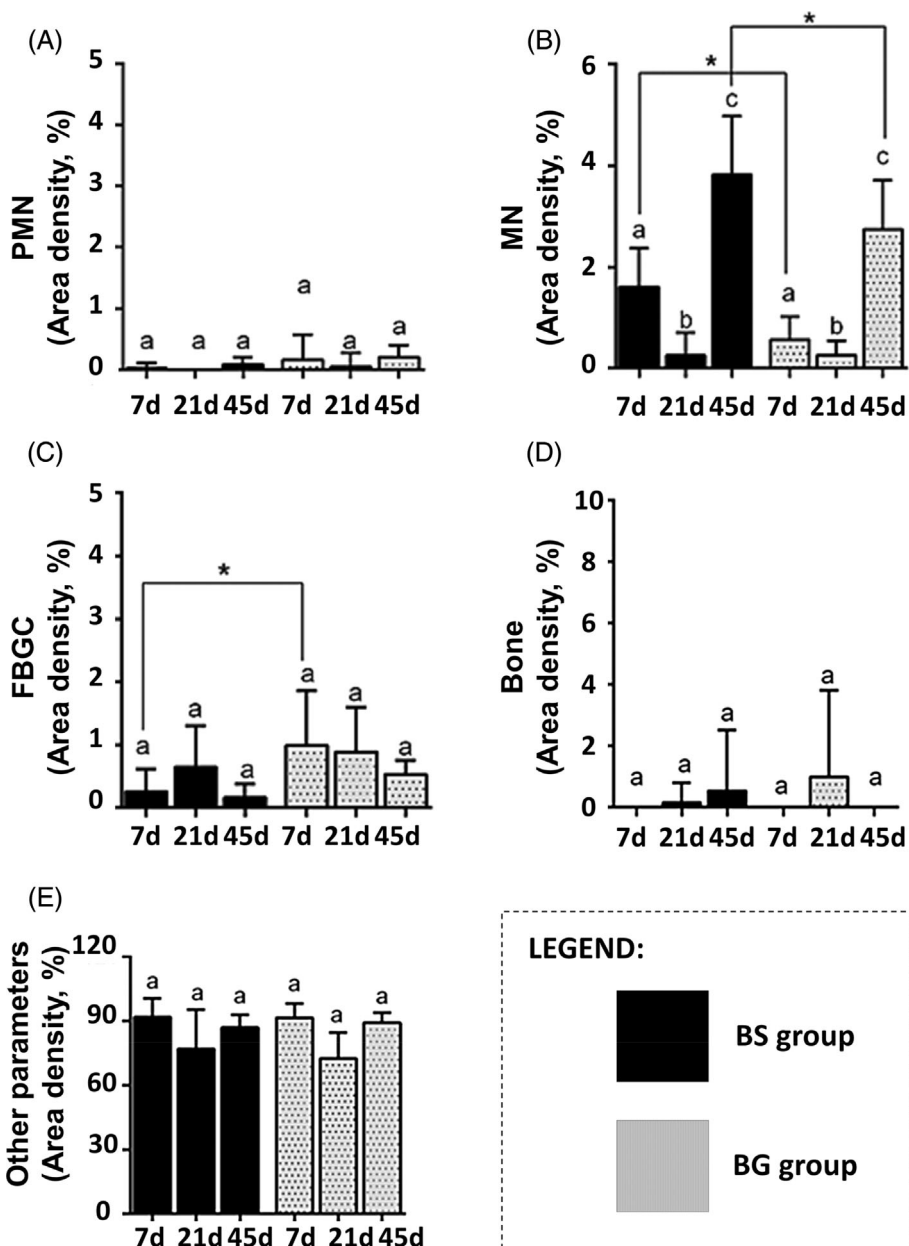


FIGURE 2 Histomorphometry analysis of inflammatory cells, bone and other parameters during bone healing defects filled with BS and BG materials. (A) No statistically significant differences were detected considering PMN between BS and BG groups in all experimental periods. (B) The area density of MN was significant higher in BS group at 45 (3.82 ± 1.16 vs. 2.74 ± 0.96 ; $p < .05$), and 7 (1.61 ± 0.76 vs. 0.56 ± 0.46 ; $p < .05$) days compared to BG group, respectively. (C) FBGCs were significant higher at 7 days in BG group (0.25 ± 0.36) compared to BS group (0.25 ± 0.36) ($p < .05$). No significant differences were found considering (D) bone density, as well as the (E) other parameters including empty spaces, and collagen fibers. Different lower-case letters indicate statistically significant differences among the periods of the same group ($p \leq .05$). Symbols (*) indicate statistically significant differences between the groups in the same experimental period. Results represent mean and SD values of each analyzed period (A - PMN, B - MN, C - FBGC, D - Biomaterial, E - Bone tissue, F - Others).

days compared to BG group, respectively (Figure 2B). On the other hand, FBGCs were significant higher at 7 days in BG group (0.99 ± 0.86) compared to BS group (0.25 ± 0.36) ($p < .05$; Figure 2C). No significant differences were found considering bone density (Figure 2D), as well as the other parameters including empty spaces, and collagen fibers (Figure 2E).

3.3 | Quantitative assessment of immunolabeled positive cells for CD206, TGF- β , and iNOS

We next investigated whether M1 and M2 related-markers regulate activities in response to glass-ceramic and bone repair. Immunostaining of CD206⁺ cells were characterized by strong and homogenous cytoplasmic positivity in both BS and BG groups. CD206⁺ cells distribution was similar among groups and period, although significant differences were observed in BS at day 45 (56.4 ± 5.02), compared to 7 (28.8 ± 3.49), and 21 (28 ± 7.25) days ($p < .05$), respectively. Also, when we compared its positivity, CD206⁺ cells were higher at 45 days of BS (56.4 ± 5.02) compared to BG (56.4 ± 5.02) group ($p < .05$; Figure 3A).

Regarding TGF- β immunostaining, it was mostly found in cytoplasm of macrophages, and FBGCs, as well as secreted among collagen fibers of BS and BG groups. However, exhibiting strong positivity in BG (20 ± 7.55) compared to BS (6.25 ± 3.30) group, being statistically significant only at period of 21 days ($p < .05$; Figure 3B). It is important to note that, BS and BG demonstrated distinct patterns at 21 days, exhibiting the lowest and the highest number of TGF- β ⁺ cells, respectively. The iNOS immunostaining was composed by moderated cytoplasmic positivity, especially around granules at period of 7 days cells, followed by decreasing at 21, and 45 days, although no significant differences were detected in the comparison of iNOS⁺ cells ($p > .05$; Figure 3C).

4 | DISCUSSION

Invasive procedures involving biomaterials often trigger a bone inflammatory response that typically promotes foreign body reactions through a dynamic process regulated by the balance between pro and anti-inflammatory molecules. Various types of resident and inflammatory cells can modulate these mechanisms to either adapt or activate the body's rejection response to the implanted biomaterial.⁴¹ Synthetic bone substitutes with the capacity to influence attachment, proliferation, differentiation, and mineralization of bone cells, while minimizing a robust pro-inflammatory reaction, hold promise for enhancing the success of procedures involving biomaterial implantation.⁴⁰ In this context, our previously published study demonstrated that BG biomaterials possess the independent capability to generate bone matrix similar to autogenous bone. Furthermore, they regulate bone remodeling by influencing the production of metalloproteinases -2 and -9 during the later stages of bone healing.⁴² Despite the successful descriptions of various glass-ceramic biomaterial compositions aimed at improving osteogenesis in numerous published studies,⁴³⁻⁴⁷

the precise roles of inflammatory cells and their direct involvement mechanisms in bone healing remain elusive.

Given the multifunctional effects of biomaterials to stimulate the osteogenic and osteoclastogenic healing processes through activation or depletion of innate (neutrophils), and adaptive (lymphocytes and plasma cells) immune inflammatory cells,^{48,49} we further investigated their presence during an experimental period of 7, 21, and 45 days after BS and BG implantation. Our findings demonstrated that the percentage of MN was higher at final periods of bone healing, followed by 7, and 21 days in BS, and BG groups implantation, suggesting a potential late involvement of adaptive immune response, especially in the BS group. More importantly, the MN area density was significantly higher in the BS group at 45, and 7 days compared to the BG group, respectively. It is known that adaptive immune response begins after innate immune response or large injuries in bone repair, compromising by a substantial number of T-helper cells, follicular T cells, B cells, and plasma cells.⁵⁰ In bone injury, T-helper cells display important functions, mainly related to promoting macrophage adhesion to the foreign body and/or supporting an anti-inflammatory environment through IL-10 and TGF- β secretion. Additionally, B lymphocytes also contribute to IL-10 production, and T cell co-stimulation.⁵¹ Despite their relevant role in bone repair, it was reported that the maintenance of lymphocytes in late periods of biomaterial implantation could induce a locally chronic inflammatory mainly related to the non-degrading biomaterial, leading to fibrotic tissue, and failure in effectiveness bone repair.⁵² Although we did not evaluate MN cells according to their subtypes or found a significant difference in collagen fibers, it was possible to note a thickening in collagen fibers of the BS group. These results suggested that BS biomaterial promoted a late hyper-regulation of MN cells, compared to the BG group, demonstrating a less effective adaptive cells recruitment regulation among periods.

Other immune cells can also display important roles in bone repair after biomaterials' implantations. The macrophages are the earliest cells that arrive to injury; these cells are derived from the bone marrow precursors, and act as regulators for the differentiation and function of osteoblasts and osteoclasts, being crucial to the healing process.⁵³ Macrophages are widely plastic in the microenvironment according to their activation and functions, being divided based on the surface markers into unpolarized (M0), pro-inflammatory phenotypes (M1), and anti-inflammatory phenotypes (M2).⁵⁴ Besides that, macrophage precursors, the monocytes, can promote membrane fusion to form FBGCs on biomaterial surfaces, being able to degrade certain types of materials.^{55,56} In this sense, we compared the differences concerning the area density of FBGCs in our groups at 7, 21, and 45 days after biomaterials implantation. Regardless of statistical significance, it is possible to observe that in the BG group FBGCs regularly decrease from 7 to 45 days, whilst in the BS group the highest density was in 21 days, being 7 and 45 days similar in FBGCs area density, suggesting different mechanisms in FBGCs activation according to biomaterial properties.

Furthermore, a significant increase of FBGCs in the BG group at day 7, compared to BS was found, demonstrating early efficient recruitment of FBGCs against sol-gel-derived glass-ceramic particulate (BG group). Despite foreign body reaction in bone sites

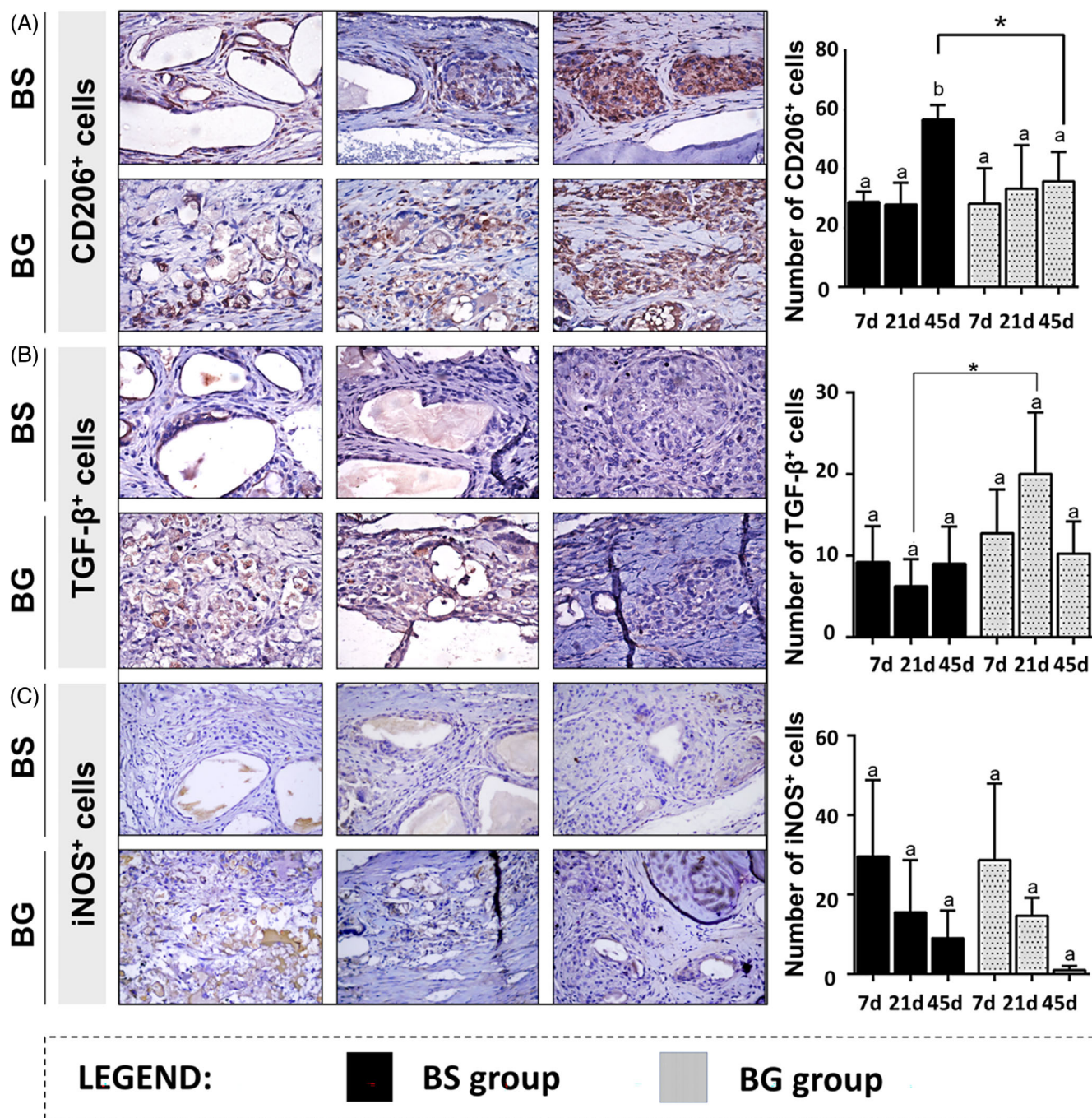


FIGURE 3 Histomorphometry characterization CD206, TGF- β , and iNOS-positive cells during bone healing defects reconstructed with BS and BG materials. (A) Immunostaining of CD206⁺ cells were characterized by strong and homogenous cytoplasmatic positivity in both BS and BG groups. CD206⁺ cells distribution was high BS at day 45 (56.4 ± 5.02), compared to 7 (28.8 ± 3.49), and 21 (28 ± 7.25) days ($p < .05$), respectively. CD206⁺ cells were also higher at 45 days of BS (56.4 ± 5.02) compared to BG (56.4 ± 5.02) group ($p < .05$). (B) TGF- β immunostaining was mostly found in cytoplasm of macrophages, and FBGCs, as well as secreted among collagen fibers of BS and BG groups, exhibiting strong positivity in BG (20 ± 7.55) compared to BS (6.25 ± 3.30) group, being statistically significant only at period of 21 days ($p < .05$). (C) The iNOS immunostaining was composed by moderated cytoplasmatic positivity, especially around granules at period of 7 days cells, followed by decreasing at 21, and 45 days, although no significant differences were detected in the comparison of iNOS⁺ cells. Different lower-case letters indicate statistically significant differences among the periods of the same group ($p \leq .05$). Symbols (*) indicate statistically significant differences between the groups in the same experimental period. Results represent mean and SD values of each analyzed period.

reconstructed with biomaterials being already considered as a failure, being related to rejection,⁵¹ in dental implants osseointegration, FBGCs have been considered as a necessary and favorable event in regulated inflammation.⁵⁷ Consistently, the architecture of biomaterial

usually requires a functional surface topography that allows macrophages to adhesion and activation, adsorb proteins, deliver molecules, and facilitate their fusion into FBGCs.⁵⁸ Noteworthy, the sol-gel processing routes require additional reagents for biomaterial

production, and it can significantly change its chemical behavior resulting in a more soluble biomaterial.⁴⁹ Altogether, our findings demonstrated that glass–ceramics produced through different routes can modulate FBGCs, being the sol–gel route more efficient in promoting their early activation in bone repair. Although imaging methods were not the focus of this investigation, it is worthy to inform that microtomographic (microCT) analysis was carried out in order to verify the presence and amount of mineralized bone matrix inside the defects, and it was observed that both biomaterials were found to facilitate bone regeneration during the final 45-day period (Figure S1), despite no significant differences were detected between the groups.

Different glass–ceramic biomaterials have been developed due to its ability to regulate pro-osteogenic and anti-osteoclastogenic cellular responses through macrophages regulation *in vitro*, and *in vivo* models. However, the exact macrophage profile recruitment during all phases of bone repair remains unclear. To answer this question, the effects of glass–ceramic biomaterials on M1 (iNOS⁺), and M2 (CD206⁺/TGF-β⁺) macrophages recruitment were further explored.⁵⁹ When the effects of the BS- and BG-biomaterials on M2 macrophage recruitment were explored, CD206 and TGF-β were distinctly observed. First, CD206⁺ macrophages enhanced at the final periods of both groups, being significantly higher in 45 days of BS compared to the BG group. Nonetheless, CD206 homogeneously increased in the BG group and was downregulated at 21 days compared to 7 days of the BS group, demonstrating different roles among groups, and periods despite statistical significance. In accordance with our findings, Li et al. demonstrated that Alpha-ketoglutarate (αKG) metabolites could continuously aggrandize CD206⁺ cells at the later healing stage, and also could transform from M1 pro-inflammatory phenotype (iNOS⁺) toward M2 anti-inflammatory phenotype during alveolar bone healing.⁶⁰

On the other hand, the density of TGF-β⁺ cells on 21 days were the highest in BG, and the lowest in the BS group, demonstrating a differential synergy among groups. Noteworthy, TGF-β⁺ cells were significantly higher at 21 days of BG compared to the BS group. These findings were consistent with our previous finding that the TGF-β⁺ cells were predominant at day 21 during the bone healing process of rat's calvaria critical defects using bioactive vitroceraic (VC), and particulate deproteinized bovine bone (DBB).³⁸ TGF-β signaling has been associated with bone formation through Runx2 induction and promoting osteogenic matrix proteins.⁶¹ More importantly, recent studies demonstrated that macrophages were induced to an M2 rather than M1 phenotype through different molecules. CD206⁺ M2 macrophages were associated with an increase in angiogenesis of bone repair,⁶² while TGF-β release act as a guide for M2 polarization, enhancing osteogenesis and angiogenesis via the TGF-β/Snail pathway.⁶³ The other interesting result was that these FBGCs were CD206⁺, especially in the BG group, attesting to their M2 profile, which was reinforced by the significant increase of TGF-β⁺ cells at day 21 in the same group. Although this study did not separate FBGCs, and macrophages according to markers labeling, and considering that release of osteogenic matrix proteins is an important step of

bone healing, and at day 21 a fracture can be healed in rat models⁶⁴ we believe that the maintenance of M2 TGF-β⁺ macrophages can induce pro-osteogenic cellular responses in BG biomaterials.

5 | CONCLUSION

Taken together, these results indicated that glass–ceramic biomaterials can act differently in the biological process of bone remodeling, demonstrating that glass–ceramic produced by the sol–gel route led to distinct inflammatory profiling in bone healing, promoting a better biomaterial degradation in comparison to the traditional route production. In addition to biomaterial properties analysis, our study reveals for the first time the glass–ceramic produced by the sol–gel route can efficiently recruit M2 macrophages and promote a specific response of bone healing.

ACKNOWLEDGMENTS

The authors acknowledge Maira Cristina Rondina Couto for her technical assistance in this study.

FUNDING INFORMATION

This work was supported by the #2016/03762-7 grant from São Paulo Research Foundation (FAPESP).

CONFLICT OF INTEREST STATEMENT

The authors declare no conflicts of interest.

DATA AVAILABILITY STATEMENT

The data that support the findings of this study are available from the corresponding author upon reasonable request.

ORCID

Mariza Akemi Matsumoto  <https://orcid.org/0000-0001-5389-0105>

REFERENCES

- Dimitriou R, Jones E, McGonagle D, Giannoudis PV. Bone regeneration: current concepts and future directions. *BMC Med.* 2011; 31(9):66.
- Bharathi R, Ganesh SS, Harini G, et al. Chitosan-based scaffolds as drug delivery systems in bone tissue engineering. *Int J Biol Macromol.* 2022;1:132-153.
- Galindo-Moreno P, Abril-García D, Carrillo-Galvez AB, et al. Maxillary sinus floor augmentation comparing bovine versus porcine bone xenografts mixed with autogenous bone graft. A split-mouth randomized controlled trial. *Clin Oral Implants Res.* 2022;33:524-536.
- Esposito M, Grusovin MG, Rees J, et al. Effectiveness of sinus lift procedures for dental implant rehabilitation: a Cochrane systematic review. *Eur J Oral Implantol.* 2010;3:7-26.
- Jakoi AM, Iorio JA, Cahill PJ. Autologous bone graft harvesting: a review of grafts and surgical techniques. *Musculoskelet Surg.* 2015;99: 171-178.
- Georgeanu VA, Gingu O, Antoniac IV, Manolea HO. Current options and future perspectives on bone graft and biomaterials substitutes for bone repair, from clinical needs to advanced biomaterials research. *Appl Sci.* 2023;13:8471.

7. Kotlarz M, Melo P, Ferreira AM, Gentile P, Dalgarno K. Cell seeding via bioprinted hydrogels supports cell migration into porous apatite-wollastonite bioceramic scaffolds for bone tissue engineering. *Biomater Adv.* 2023;21:213532.
8. Granito RN, Rennó AC, Ravagnani C, et al. In vivo biological performance of a novel highly bioactive glass-ceramic (Biosilicate®): a biomechanical and histomorphometric study in rat tibial defects. *J Biomed Mater Res B Appl Biomater.* 2011;97:139-147.
9. Ben-Arfa BAE, Pullar RC. A comparison of bioactive glass scaffolds fabricated by robocasting from powders made by sol-gel and melt-quenching methods. *Processes.* 2020;8:615.
10. Barberi J, Bairo F, Fiume E, et al. Robocasting of SiO₂-based bioactive glass scaffolds with porosity gradient for bone regeneration and potential load-bearing applications. *Materials.* 2019;12:2691.
11. Fiume E, Schiavi A, Orlygsson G, Bignardi C, Verné E, Bairo F. Comprehensive assessment of bioactive glass and glass-ceramic scaffold permeability: experimental measurements by pressure wave drop, modelling and computed tomography-based analysis. *Acta Biomater.* 2021;1:405-418.
12. Bairo F, Barberi J, Fiume E, Orlygsson G, Massera J, Verné E. Robocasting of bioactive SiO₂-P₂O₅-CaO-MgO-Na₂O-K₂O glass scaffolds. *J Health Eng.* 2019;11:5153136.
13. Fiume E, Bairo F. Robocasting of mesoporous bioactive glasses (MBGs) for bone tissue engineering. In: Osaka A, Narayan R, eds. *Elsevier Series on Advanced Ceramic Biomaterials. Bioceramics.* Vol 1. Elsevier; 2021:327-349.
14. Fiume E, Massera J, D'Ambrosio VE, Bairo F. Robocasting of multi-component sol-gel-derived silicate bioactive glass scaffolds for bone tissue engineering. *Ceram Int.* 2022;48:35209-35216.
15. Ferraz MP. Bone grafts in dental medicine: an overview of autografts, allografts and synthetic materials. *Materials.* 2023;16:4117.
16. Boesel LF, Mano JF, Reis RL. Optimization of the formulation and mechanical properties of starch based partially degradable bone cements. *J Mater Sci Mater Med.* 2004;15:73-83.
17. Pal A, Das Karmakar P, Vel R, Bodhak S. Synthesis and characterizations of bioactive glass nanoparticle-incorporated triblock copolymeric injectable hydrogel for bone tissue engineering. *ACS Appl Bio Mater.* 2023;20(6):445-457.
18. Mahato A, Kundu B, Mukherjee P, Nandi SK. Applications of different bioactive glass and glass-ceramic materials for osteoconductivity and osteoinductivity. *Trans Indian Ceram.* 2017;76:149-158.
19. Thompson ID, Hench LL. Mechanical properties of bioactive glasses, glass-ceramics and composites. *Proc Inst Mech Eng H.* 1998;212:127-136.
20. Arcos D, Vallet-Regí M. Sol-gel silica-based biomaterials and bone tissue regeneration. *Acta Biomater.* 2010;6:2874-2888.
21. Fiume E, Massera J, D'Ambrosio D, Verné E, Bairo F. Robocasting of multicomponent sol-gel-derived silicate bioactive glass scaffolds for bone tissue engineering. *Ceramics Int.* 2022;48:35209-35216.
22. Gupta R, Kumar A. Bioactive materials for biomedical applications using sol-gel technology. *Biomed Mater.* 2008;3:034005.
23. Siqueira RL, Zanotto ED. The influence of phosphorus precursors on the synthesis and bioactivity of SiO₂-CaO-P₂O₅ sol-gel glasses and glass-ceramics. *J Mater Sci Mater Med.* 2013;24:365-379.
24. Palmer JA, Abberton KM, Mitchell GM, Morrison WA. Macrophage phenotype in response to implanted synthetic scaffolds: an immunohistochemical study in the rat. *Cells Tissues Organs.* 2014;199:169-183.
25. Altieri DC, Mannucci PM, Capitanio AM. Binding of fibrinogen to human monocytes. *J Clin Invest.* 1986;78:968-976.
26. Wynn TA, Vannella KM. Macrophages in tissue repair, regeneration, and fibrosis. *Immunity.* 2016;44:450-462.
27. Zaveri TD, Lewis JS, Dolgova NV, Clare-Salzler MJ, Keselowsky BG. Integrin-directed modulation of macrophage responses to biomaterials. *Biomaterials.* 2014;35:3504-3515.
28. Fujiwara N, Kobayashi K. Macrophages in inflammation. *Curr Drug Targets Inflamm Allergy.* 2005;4:281-286.
29. Sridharan R, Cameron AR, Kelly DJ, Kearney CJ, O'Brien FJ. Biomaterial based modulation of macrophage polarization: a review and suggested design principles. *Mater Today.* 2015;18:313-325.
30. Mosser DM. The many faces of macrophage activation. *J Leukoc Biol.* 2003;73:209-212.
31. Mosser DM, Edwards JP. Exploring the full spectrum of macrophage activation. *Nat Rev Immunol.* 2008;8:958-969.
32. Koh TJ, DiPietro LA. Inflammation and wound healing: the role of the macrophage. *Expert Rev Mol Med.* 2011;13:e23.
33. Xia Z, Triffitt JT. A review on macrophage responses to biomaterials. *Biomed Mater.* 2006;1:R1-R9.
34. Moreno JL, Mikhailenko I, Tondravi MM, Keegan AD. IL-4 promotes the formation of multinucleated giant cells from macrophage precursors by a STAT6-dependent, homotypic mechanism: contribution of E-cadherin. *J Leukoc Biol.* 2007;82:1542-1553.
35. Christo SN, Diener KR, Bachhuka A, Vasilev K, Hayball JD. Innate immunity and biomaterials at the nexus: friends or foes. *Biomed Res Int.* 2015;2015:342304.
36. Trindade R, Albrektsson T, Wennerberg A. Current concepts for the biological basis of dental implants: foreign body equilibrium and osseointegration dynamics. *Oral Maxillofac Surg Clin North Am.* 2015;27:175-183.
37. Siqueira RL, Alano JH, Peitl O, Zanotto ED. Glass Panacea: a user-friendly free software tool for the formulation of glasses, glass-ceramics, and ceramics. *Am Ceram Soc Bull.* 2017;96:48-49.
38. Munerato MS, Bigueti CC, Parra da Silva RB, et al. Inflammatory response and macrophage polarization using different physicochemical biomaterials for oral and maxillofacial reconstruction. *Mater Sci Eng C Mater Biol Appl.* 2020;107:110229.
39. Bigueti CC, De Oliva AH, Healy K, et al. Medication-related osteonecrosis of the jaws after tooth extraction in senescent female mice treated with zoledronic acid: microtomographic, histological and immunohistochemical characterization. *PLoS One.* 2019;14:e0214173.
40. Amini AR, Laurencin CT, Nukavarapu SP. Bone tissue engineering: recent advances and challenges. *Crit Rev Biomed Eng.* 2012;40:363-408.
41. Marques AP, Reis RL, Hunt JA. The biocompatibility of novel starch-based polymers and composites: in vitro studies. *Biomaterials.* 2002;23:1471-1478.
42. Bigueti CC, Cavalla F, Tim CR, et al. Bioactive glass-ceramic bone repair associated or not with autogenous bone: a study of organic bone matrix organization in a rabbit critical-sized calvarial model. *Clin Oral Investig.* 2019;23:413-421.
43. Li R, Clark AE, Hench LL. An investigation of bioactive glass powders by sol-gel processing. *J Appl Biomater.* 1991;2:231-239.
44. Vallet-Regí M, Rangel VR, Salinas AJ. Glasses with medical applications. *Eur J Inorg Chemistry.* 2003;2002:1029-1042.
45. Vichery C, Nedelec JM. Bioactive glass nanoparticles: from synthesis to materials design for biomedical applications. *Materials.* 2016;9:288.
46. Jones JR, Ehrenfried LM, Hench LL. Optimising bioactive glass scaffolds for bone tissue engineering. *Biomaterials.* 2006;27:964-973.
47. Jones JR. New trends in bioactive scaffolds: the importance of nanostructure. *J Eur Ceram Soc.* 2009;29:1275-1281.
48. Sun JS, Lin FH, Hung TY, Tsuang YH, Chang WH, Liu HC. The influence of hydroxyapatite particles on osteoclast cell activities. *J Biomed Mater Res.* 1999;45:311-321.
49. Hotchkiss KM, Clark NM, Olivares-Navarrete R. Macrophage response to hydrophilic biomaterials regulates MSC recruitment and T-helper cell populations. *Biomaterials.* 2018;182:202-215.
50. Balaji S, Cholan PK, Victor DJ. An emphasis of T-cell subsets as regulators of periodontal health and disease. *J Clin Transl Res.* 2021;7:648-656.
51. Könnecke I, Serra A, El Khassawna T, et al. T and B cells participate in bone repair by infiltrating the fracture callus in a two-wave fashion. *Bone.* 2014;64:155-165.

52. Boehler RM, Graham JG, Shea LD. Tissue engineering tools for modulation of the immune response. *Biotechniques*. 2011;51:239-240, 242, 244.
53. Kitagawa Y, Ohkura N, Sakaguchi S. Molecular determinants of regulatory T cell development: the essential roles of epigenetic changes. *Front Immunol*. 2013;4:106.
54. Rees AJ. Monocyte and macrophage biology: an overview. *Semin Nephrol*. 2010;30:216-233.
55. Yagi M, Miyamoto T, Sawatani Y, et al. DC-STAMP is essential for cell-cell fusion in osteoclasts and foreign body giant cells. *J Exp Med*. 2005;202:345-351.
56. Dittmar T, Zänker KS. Cell fusion in health and disease. Volume II: cell fusion in disease. Introduction. *Adv Exp Med Biol*. 2011;714:1-3.
57. Albrektsson T, Dahlin C, Jemt T, Sennerby L, Turri A, Wennerberg A. Is marginal bone loss around oral implants the result of a provoked foreign body reaction? *Clin Implant Dent Relat Res*. 2014;16:155-165.
58. Tripathy N, Perumal E, Ahmad R, Song JE, Khang G. Hybrid composite biomaterials. In: Atala A, Lanza R, Miko AG, Nerem R, eds. *Principles of Regenerative Medicine*. Academic Press; 2019:695-714.
59. Martinez FO, Helming L, Gordon S. Alternative activation of macrophages: an immunologic functional perspective. *Annu Rev Immunol*. 2009;27:451-483.
60. Li Y, Liu L, Li Y, et al. Alpha-ketoglutarate promotes alveolar bone regeneration by modulating M2 macrophage polarization. *Bone Rep*. 2023;18:101671.
61. Kasagi S, Chen W. TGF-beta1 on osteoimmunology and the bone component cells. *Cell Biosci*. 2013;3:4.
62. Han X, Hu J, Zhao W, Lu H, Dai J, He Q. Hexapeptide induces M2 macrophage polarization via the JAK1/STAT6 pathway to promote angiogenesis in bone repair. *Exp Cell Res*. 2022;413:113064.
63. Li D, Yang Z, Zhao X, et al. Osteoimmunomodulatory injectable Lithium-Heparin hydrogel with Microspheres/TGF- β 1 delivery promotes M2 macrophage polarization and osteogenesis for guided bone regeneration. *Chem Eng J*. 2022;435:134991.
64. Li J, Ahmad T, Spetea M, Ahmed M, Kreicbergs A. Bone reinnervation after fracture: a study in the rat. *J Bone Miner Res*. 2001;16:1505-1510.

SUPPORTING INFORMATION

Additional supporting information can be found online in the Supporting Information section at the end of this article.

How to cite this article: da Silva RBP, Biguetti CC, Munerato MS, et al. Effects of glass-ceramic produced by the sol-gel route in macrophages recruitment and polarization into bone tissue regeneration. *J Biomed Mater Res*. 2023;1-10. doi:[10.1002/jbm.b.35340](https://doi.org/10.1002/jbm.b.35340)